Conf-9209174--1

CONF-9209174--1

DE92 017813

# Shallow-Crack Toughness Results for Reactor Pressure Vessel Steel

T. J. Theiss MS Oak Ridge National Laboratory
S. T. Rolfe PhD, P. E. University of Kansas
D. K. M. Shum PhD Oak Ridge National Laboratory

## SUMMARY

The Heavy Section Steel Technology Program (HSST) is investigating the influence of flaw depth on the fracture toughness of reactor pressure vessel (RPV) steel. To complete this investigation, techniques were developed to determine the fracture toughness from shallow-crack specimens. A total of 38 deep and shallow-crack tests have been performed on beam specimens about 100 mm deep loaded in 3-point bending. Two crack depths ($a \approx 50$ and 9 mm) and three beam thicknesses ($B \approx 50$, 100, and 150 mm) have been tested. Techniques were developed to estimate the toughness in terms of both the J-integral and crack-tip opening displacement (CTOD). Analytical J-integral results were consistent with experimental J-integral results, confirming the validity of the J-estimation schemes used and the effect of flaw depth on fracture toughness. Test results indicate a significant increase in the fracture toughness associated with the shallow flaw specimens in the lower transition region compared to the deep-crack fracture toughness. There is, however, little or no difference in toughness on the lower shelf where linear-elastic conditions exist for specimens with either deep or shallow flaws. The increase in shallow-flaw toughness compared with deep-flaw results appears to be well characterized by a temperature shift of 35°C.

## INTRODUCTION

The Heavy-Section Steel Technology (HSST) program sponsored by the U. S. Nuclear Regulatory Commission (NRC), is investigating the influence of crack depth on the fracture toughness of A533B material under conditions prototypic of a pressurized-water reactor (PWR) vessel. Specifically, HSST is quantifying the magnitude of the increase in fracture toughness associated with shallow rather than deep-flaw specimens. The shallow-flaw fracture toughness increase (i.e. shallow-flaw effect) is due to a loss of constraint at the crack-tip because of the proximity of the crack-tip to the specimen surface. This paper presents the final toughness results from the HSST shallow-crack fracture toughness testing program, posttest analysis, and interpretation of the results. More detailed information on the motivation and objectives of the program, experimental set-up, and verification of the test techniques used can be found in previously published reports by Theiss et al (1-4).

The HSST shallow-flaw program is a joint experimental/analytical program which has produced a limited data base of shallow-flaw fracture toughness values and analysis to aid in the transferability of the specimen data to an RPV. The experimental portion of the program was divided into two phases: a development phase and a production phase. The development phase established the techniques appropriate for shallow-crack testing, verified the existence of a shallow-flaw effect in A533B beams, and compared beams of three thicknesses to choose the thickness for the production phase of the program. Broken ends of the development phase beams were subsequently remachined and tested yielding six additional deep-crack beam tests. The production phase of the experimental portion of the program developed a limited data base of shallow-crack toughness values at various temperatures. The analytical portion of the shallow-flaw program conducted pretest and posttest analyses of the test specimens. The pretest analysis was used to size the instrumentation for the tests and select an appropriate shallow-crack depth. Posttest analysis verified the techniques developed to determine the toughness for the shallow-crack specimens and quantified the constraint in the deep- and shallow-crack test specimens.

## EXPERIMENTAL PROGRAM

The specimen configuration chosen for all testing in the shallow-crack program is the single-edge-notch-bend (SENB) specimen with a through-thickness crack (as opposed to the 3D surface crack). A beam approximately 100-mm-deep (W) was selected for use in the HSST shallow-crack project. To maintain consistency with ASTM standards, the beams were tested in three-point bending. All testing was conducted on unirradiated reactor material (A533 Grade B, Class 1 steel) with the cracks oriented in the thickness (S) direction to simulate the material conditions of an axial flaw in an RPV. Specimens were taken from the centre, homogeneous region of the source plate to prevent metallurgical differences between the material surrounding a shallow and deep flaw from influencing the toughness result.

The specimen thickness was varied in the development phase tests to examine the influence of thickness on toughness. Three beam thicknesses were used: B ≈ 50, 100, and 150 mm. The span (S) for the 50-mm-thick beam was 4W or 406 mm. The spans for the 100- and 150-mm beams were increased to assure failure without exceeding the load capacity of the beam fixture. Figure 1 shows three of the beam sizes used in the shallow-crack testing. Both shallow- and deep-crack specimens were tested at each thickness. Beams 100 mm thick were used for the production phase tests.

The development and production phases of the HSST shallow-crack testing program resulted in 14 and 18 data points, respectively. In addition, 6 deep-crack beams of varying thickness were tested yielding a data base of 38 specimens. The development phase tests were conducted primarily at -60°C using beams of three different thicknesses. The 6 additional deep-crack beams were tested at -45°C using beams with different thicknesses. The production phase tests used one beam geometry (100 x 100 mm) but were conducted at various temperatures. Two crack depths (one shallow and one deep) were tested during the shallow-crack fracture toughness testing program. The nominal shallow crack depth chosen was a ≈ 10 mm, which was representative of the flaw depth of interest for RPVs as discussed by Cheverton et al (5) and yields a normalized crack depth a/W of 0.10. All deep-crack specimens were cracked to an a/W ratio of approximately 0.5.

Instrumentation was attached to the specimens to make both J-integral and crack-tip opening displacement (CTOD) measurement of fracture toughness. The J-integral was determined from the load-line-displacement (LLD) using a reference bar attached to the beam fixture and a micrometer attached to the neutral axis of the beam. CTOD was determined from crack-mouth-opening-displacement (CMOD) using clip gages mounted directly on the crack mouth of the specimen. Toughness data are expressed in terms of CTOD according to ASTM E1290-89, Crack-Tip Opening Displacement (CTOD) Fracture Toughness Measurement. ASTM E399, Plane-Strain Fracture Toughness of Metallic Materials, was used to analyze the deep-crack specimens to determine if the test results could be considered "valid" plane-strain ($K_{Ic}$) data. ASTM E813, $J_{Ic}$, A Measure of Fracture Toughness, is not strictly applicable to these tests since typically the failures were cleavage events; however, critical J-integral cleavage values ($J_c$) were determined for each test. The shallow-crack toughness formulations are as similar as possible to the deep-crack ASTM standard toughness formulations.

### Material Properties

Two heats of unirradiated A 533 B material were tested in this program. The development phase and six additional deep-crack beams were taken from the HSST-CE plate and were tested in the T-S orientation. The production phase beams were taken from HSST Plate 13B, given a final heat treatment prior to machining and tested in the L-S orientation. Material properties used in the analysis of the shallow-crack test results for both the development and production phases are included in Table 1. Additional information on the shallow-crack production-phase material characterization is being published by Iskander* and material properties of the source plates have been reported by Naus et al (6) & (7).

---

* S. K. Iskander, "Preliminary Report on the Characterization of HSST Plate 13B in the L-S Orientation," to be issued as a USNRC NUREG report.

**Table 1 Material properties for A 533 B steels used in HSST shallow-crack program**

| *Development phase and six deep-crack beams* | *Production phase* |
|---|---|
| HSST CE–WP | HSST Plate 13B after postweld heat treatment |
| $E = 202 - 0.0626\ T$, GPa | $E = 202 - 0.0626\ T$, GPa |
| $\nu = 0.3$ | $\nu = 0.3$ |
| $\sigma_0 = 211 + 55{,}000 / (T + 273)$, MPa | $\sigma_0 = 430 - 0.223\ T + 0.014\ T^2$, MPa |
| $\sigma_u = 371 + 55{,}000 / (T + 273)$, MPa | $\sigma_u = 609 + 0.618\ T + 0.00927\ T^2$, MPa |
| $\sigma_f = 1/2\ (\sigma_0 + \sigma_u)$ | $\sigma_f = 1/2\ (\sigma_0 + \sigma_u)$ |
| $RT_{NDT} = -35°C$ | $RT_{NDT} = -15°C$ (centre material) |

T = temperature, °C.

## Crack Tip Opening Displacement (CTOD), $\delta_c$, Determination

According to ASTM E1290, the plastic component of CTOD is determined experimentally from the plastic component of CMOD and the rotation factor (RF). The plastic displacement of the crack flanks is assumed to vary linearly with distance from the plastic centre of rotation. In this way, the plastic CMOD can be related to the plastic CTOD. The plastic centre of rotation is located ahead of the crack tip a distance equal to the rotation factor multiplied by the remaining ligament (W-a). The rotation factor in ASTM E1290 is given to be 0.4, but is a function of specimen geometry and material. Rotation factor values determined for deep-crack beams are not necessarily appropriate for otherwise identical shallow-crack beams.

An experimental technique was utilized in this program to locate the neutral axis of the beam ahead of the crack tip using strain gages on each face of the beam. Assuming the plastic centre of rotation is located at the neutral axis of the beam, the RF can be determined. Since the rotation factor relates the plastic component of CMOD to the plastic component of CTOD, only plastic strains were used to determine the rotation factor. The rotation factors determined using this technique were relatively insensitive to load once plastic strains became nontrivial and were consistent on each face of the beam. The RF for a beam was taken as the average calculated RF from each face. Four deep-crack beams were strain gaged yielding an average RF of 0.44. Eight shallow-crack beams were gaged to yield an average RF of 0.49. The rotation factor used for the CTOD toughness calculation is the average of the values from this technique for the two crack depths.

A parametric evaluation was performed to assess the sensitivity of the RF upon the calculated CTOD toughness. This evaluation indicated that the plastic component of CTOD is not overly sensitive to the value of the rotation factor. Shallow-crack beams are less sensitive to the rotation factor than deep-crack beams. A 25% increase in rotation factor increases the plastic CTOD by about 5% and 17% for the shallow and deep-crack geometries, respectively. The rotation factor is insensitive to beam thickness and absolute beam dimensions, varying only with a/W ratios for a given material and specimen depth. Based on the comparison of deep and shallow RF and the relative insensitivity of CTOD to RF, the ASTM E1290 value of the RF of 0.4 would appear to be appropriate for both deep and shallow-cracked A533B specimens.

Critical CTOD toughness ($\delta_c$) values calculated using the RF values just described and ASTM E1290-89 are included in Table 2. The ratios of the shallow-to-deep lower bound $\delta_c$ at T-$RT_{NDT}$ of -25°C and -10°C are 3.3 and 4.9 respectively which is consistent with the A36 and A517 results published by Sorem et al (8) and Smith & Rolfe (9), respectively from the University of Kansas. Further examination of these data indicate little variation of $\delta_c$ as a function of beam thickness for either the deep-crack or shallow-crack beams.

**Table 2 HSST shallow-crack test data**

| HSST beam No. | Temperature (°C) | S (mm) | B (mm) | W (mm) | a (mm) | Failure load (kN) | CTOD total (mm) | J integral (MPa-mm) | $K_c$ from CTOD (MPa•$\sqrt{m}$) | $K_c$ from J (MPa•$\sqrt{m}$) |
|---|---|---|---|---|---|---|---|---|---|---|
| | | | | | *Development phase* | | | | | |
| 3 | –36 | 406 | 51 | 100 | 10.0 | 600.0 | 0.586 | 261 | 265 | 243 |
| 4 | –61 | 406 | 51 | 100 | 51.8 | 128.1 | 0.048 | 42 | 96 | 97 |
| 5 | –55 | 406 | 51 | 99 | 51.2 | 139.7 | 0.049 | 48 | 97 | 105 |
| 6 | –59 | 406 | 51 | 100 | 51.9 | 184.6 | 0.117 | 102 | 149 | 152 |
| 7 | –59 | 406 | 51 | 94 | 10.2 | 483.5 | 0.137 | 92 | 132 | 144 |
| 8 | –60 | 406 | 51 | 94 | 9.6 | 657.4 | 0.476 | 284 | 245 | 254 |
| 9 | –62 | 406 | 51 | 94 | 9.5 | 552.4 | 0.352 | 173 | 212 | 198 |
| 10 | –60 | 406 | 51 | 94 | 14.0 | 489.3 | 0.235 | 143 | 180 | 180 |
| 11 | –57 | 864 | 102 | 94 | 8.4 | 472.4 | 0.196 | 101 | 157 | 152 |
| 12 | –57 | 864 | 102 | 95 | 49.8 | 116.5 | 0.061 | 50 | 108 | 106 |
| 13 | –60 | 864 | 102 | 94 | 8.8 | 501.7 | 0.357 | 208 | 213 | 217 |
| 14 | –60 | 864 | 152 | 93 | 8.7 | 723.2 | 0.346 | 225 | 209 | 226 |
| 15 | –59 | 864 | 153 | 94 | 8.7 | 684.1 | 0.146 | 85 | 136 | 139 |
| 16 | –58 | 864 | 153 | 94 | 50.0 | 170.4 | 0.060 | 46 | 107 | 102 |
| | | | | | *Six deep-crack beams phase* | | | | | |
| 12A | –44 | 406 | 102 | 94 | 51.0 | 251.8 | 0.077 | 60 | 120 | 117 |
| 13A | –46 | 406 | 102 | 94 | 50.8 | 293.1 | 0.111 | 86 | 144 | 140 |
| 14A1 | –44 | 406 | 51 | 93 | 50.2 | 135.2 | 0.121 | 93 | 150 | 145 |
| 14A2 | –44 | 406 | 51 | 93 | 50.8 | 102.7 | 0.043 | 39 | 90 | 94 |
| 15A | –47 | 406 | 153 | 94 | 50.7 | 435.0 | 0.096 | 79 | 133 | 134 |
| 16A | –43 | 406 | 153 | 94 | 51.9 | 348.3 | 0.062 | 51 | 107 | 108 |
| | | | | | *Production phase* | | | | | |
| 17 | –6 | 610 | 102 | 102 | 52.6 | 245.1 | 0.116 | 98 | 144 | 147 |
| 18 | –24 | 610 | 101 | 102 | 10.6 | 777.1 | 0.468 | 238 | 239 | 231 |
| 20 | –4 | 610 | 101 | 101 | 10.8 | 823.3 | 1.733 | 987 | 453 | 469 |
| 21 | –23 | 610 | 101 | 102 | 10.7 | 724.1 | 0.306 | 152 | 194 | 185 |
| 22 | –7 | 610 | 101 | 102 | 10.9 | 793.5 | 0.942 | 566 | 334 | 355 |
| 24 | –7 | 610 | 102 | 102 | 52.0 | 269.1 | 0.367 | 270 | 255 | 245 |
| 25 | –39 | 610 | 102 | 102 | 52.0 | 238.4 | 0.110 | 85 | 145 | 138 |
| 26 | –40 | 610 | 102 | 102 | 11.0 | 740.1 | 0.355 | 175 | 213 | 199 |
| 27 | –22 | 610 | 101 | 102 | 10.7 | 787.3 | 0.559 | 242 | 261 | 233 |
| 28 | –6 | 610 | 101 | 102 | 10.3 | 832.7 | 1.242 | 788 | 384 | 419 |
| 31 | –40 | 610 | 102 | 102 | 51.5 | 205.5 | 0.063 | 51 | 110 | 108 |
| 32 | –103 | 610 | 102 | 102 | 11.1 | 417.7 | 0.016 | 20 | 69 | 68 |
| 33 | –103 | 610 | 102 | 102 | 10.7 | 339.8 | 0.009 | 13 | 53 | 54 |
| 34 | –106 | 610 | 101 | 102 | 10.4 | 431.0 | 0.017 | 21 | 72 | 70 |
| 35 | –7 | 610 | 102 | 102 | 51.7 | 244.2 | 0.121 | 97 | 147 | 147 |
| 36 | –38 | 610 | 102 | 102 | 51.6 | 176.1 | 0.042 | 35 | 89 | 89 |
| 37 | –39 | 610 | 102 | 102 | 10.8 | 745.9 | 0.263 | 135 | 183 | 175 |
| 38 | –39 | 610 | 102 | 102 | 10.8 | 755.3 | 0.206 | 106 | 162 | 155 |

## J-Integral, $J_c$, Determination

J-integral fracture toughness ($J_c$) was determined for each beam using LLD data. Little or no crack growth took place in these tests so ASTM E813 was not strictly applicable. The technique used to calculate the J-integral divides the elastic and plastic components of J and uses only the plastic area under the load v. LLD curve and a plastic $\eta$ factor as presented by Sumpter (10). The equations used to determine the shallow-crack J-integral toughness are as follows :

$J_c \doteq J_{el} + J_{pl}$

where [1]

$$J_{el} = K_c^2(1-\nu^2) / E \quad \text{and} \qquad [2]$$

$$J_{pl} = \eta_{pl} U_{pl} / (B(W-a)) \qquad [3]$$

where $U_{pl}$ is plastic area under load v. LLD curve.

The J-integral toughness values for each beam are given in Table 2. J-integral results are consistent with the CTOD results. The ratios of the shallow-to-deep lower bound $J_c$ at T-$RT_{NDT}$ of -25°C and -10°C are 2.4 and 2.9 respectively, which is consistent with the $\delta_c$ results.

## Comparison of $\delta_c$ and $J_c$ Values

CTOD toughness values can be converted into J-integral values as discussed by Barsom and Rolfe (11) according to $J_c = m \cdot \sigma_f \cdot \delta_c$, where $\sigma_f$ (flow strength) is the average of the yield and tensile strengths, and m is the constraint parameter. Since $J_c$ and $\delta_c$ are known for each specimen, comparison of $J_c$ and $\delta_c$ allows m to be determined as a function of crack depth. Plots of J v. CTOD show a linear relationship between the two toughness expressions. The constraint parameter, m, for each test was determined using the critical toughness ($J_c$ and $\delta_c$) values. The constraint parameter as a function of crack depth yields repeatable results as shown in Fig. 2. The average deep-crack constraint parameter value is 1.5. The average shallow-crack constraint parameter value is 1.0 except for three beams which resulted in a significantly elevated m value. These three shallow-crack beams were tested on the lower shelf where linear-elastic behaviour takes place regardless of the crack depth. An average constraint parameter value of 1.9 was found for these beams. These constraint parameter values are consistent with published results of Kirk & Dodds (12). Critical CTOD was converted into J-integral expressions using the average values of m shown in Fig. 2. J-integral values converted from CTOD will be referred to as $J_c$ (CTOD); $J_c$ (LLD) refers to J-integral values determined directly from LLD records.

## Stress-Intensity Factor, $K_c$, Determination

Typically RPV fracture toughness values are expressed in terms of the critical stress-intensity factor, $K_c$. The two J-integral toughness expressions were converted into elastic-plastic $K_c$ values according to $K_c = \sqrt{(J\,E')}$, where $E' = E / (1-\nu^2)$. The plane-strain value of E' is justified because thickness had little influence on the resulting toughness values. Figure 3 and Table 2 contain comparisons of $K_c$ from the two J estimation techniques used (CTOD and LLD). As shown in Fig. 3, the two J estimation techniques give similar values of $K_c$. The maximum difference between the two techniques is about 10%. The averaged difference is less than 1%.

The toughness data expressed in terms of $K_c$ (CTOD) vs. normalized temperature (T-$RT_{NDT}$) are presented in Table 2 and Fig. 4. The data show a significant increase in the fracture toughness for shallow-crack specimens in the transition region of the A533B toughness curve. All of the specimens failed in cleavage except the data point indicated in Fig. 4 with the arrow. As expected, the shallow-crack specimens on the lower shelf where linear-elastic behaviour occurs showed little to no toughness increase. The specimens had crack depths which were deep (a ≈ 50 mm) or shallow (a ≈ 10 mm) except for one beam with a crack depth of 14 mm. This intermediate crack-depth specimen also appears to show the shallow crack toughness elevation.

The shallow-crack toughness increase can be quantified in terms of a ratio of toughness values at one temperature or a temperature shift. In terms of $K_c$, the shallow-crack toughness increase is approximately 60% at T-$RT_{NDT}$≈ -25°C. Figure 4 shows the shallow-crack and deep-crack test data with approximate lower bound curves. The shallow-crack lower-bound curve was formed

using the deep-crack lower bound curve shifted by 35°C. The shifted deep-crack lower-bound curve fits the shallow-crack data well at all test temperatures.

Toughness data in terms of $K_c$ (CTOD) are plotted as a function of beam thickness for all of the tests conducted at T - $RT_{NDT} \approx$ -25°C and -11°C in Fig. 5. As indicated in Figs. 4 and 5, the toughness values for the shallow- and deep-crack specimens from the 100- and 150-mm-thick beams generally are consistent with the 50-mm-thick data. However, there appears to be slightly more data scatter associated with the 50-mm-thick beams than with the 100- and 150-mm-thick beams. None of the deep-crack tests strictly meet the requirements of ASTM E399 for a valid plane-strain $K_{IC}$ result due to insufficient crack depth. The beams which had otherwise linear-elastic test records and were sufficiently thick for valid results are marked in Fig. 5.

## POSTTEST SPECIMEN ANALYSIS

Detailed finite-strain, finite element analyses were performed for six specimens that were tested at -40°C. Three of the specimens (Beams # 36, 31, & 25) are deep-flaw specimens with nominal crack-depth to specimen-width ratio a/W = 0.5, while the remaining three are shallow-flaw specimens (Beams # 38, 37, & 21) with nominal a/W = 0.1. One of the primary objectives of these analyses was to evaluate the J estimation techniques developed to determine shallow-crack toughness. Additional details of the posttest analysis are discussed by Theiss et al (4).

### Material Models

Two material models have been adopted in the analysis of the test specimens. The first material model known as the unadjusted model simulates the unirradiated tensile properties of A533B (HSST Plate 13B) at -40°C as determined from limited material characterization. The unadjusted model assumed a value of E = 207.5 GPa and a uniaxial yield stress of 454 MPa. The unadjusted material model underestimated the experimentally measured displacements of the specimens. The second model known as the adjusted model was used to reduce the stiffness of the unadjusted material model based on comparisons with measured values by reducing both the Young's modulus and the uniaxial yield stress from their pretest characterization values. The magnitudes of the reductions were consistent with scatter in tensile material properties. Within the linear-elastic region the Young's modulus was reduced by 5% such that E = 196.5 GPa. The yield stress was reduced by 9% such that $\sigma_0$ = 413 MPa.

### Finite Element Models and Analyses Assumptions

The finite-strain, elastic-plastic posttest analyses are performed using the finite element code ABAQUS (13). The analyses assume a rate-independent, $J_2$ (isotropic-hardening) incremental plasticity theory as implemented in ABAQUS. The planform for both the shallow- and deep-flaw specimen is 102 mm x 610 mm. The initial flaw-depth is 10.2 mm for the shallow-flaw specimen and 50.8 mm for the deep-flaw specimen. The shallow-flaw specimen geometry is modeled with the finite element mesh, which is made up of 914 10-node generalized-plane-strain isoparametric elements with a total of 2883 nodes. The deep-flaw specimen geometry is modeled with the finite element similarly refined mesh made up of 922 10-node generalized-plane-strain isoparametric elements with a total of 2903 nodes. These 10-node elements behave as conventional 8-node isoparametric elements except for an extra degree-of-freedom (DOF) that allows for uniform straining in a direction perpendicular to the plane of the mesh (13). In a plane strain analysis the out-of-plane DOF is not active. The integration order of the elements is 2x2.

J-integral values were determined from up to 29 (shallow-flaw) or 31(deep-flaw) paths surrounding the crack tip to verify path independence. A measure of the mesh refinement is that the elastically determined K value using these meshes was within 99.5% of the value reported by Tada (14). Convergence requirements of the elastic-plastic finite element results to be presented were specified by means of limiting the maximum value of the residual nodal force per unit thickness at any node.

## Comparison of Calculated and Measured Mechanical Responses

Experimental measurements for the load (P), LLD and CMOD are available for the six specimens considered in these analyses. Comparison of the calculated values and experimental data provides a means to gage the general accuracy of the analysis results, and provide an additional basis for establishing confidence in the estimates of the fracture toughness. Results of the comparison are detailed by Theiss et al (4). As an example, Fig. 6 indicates the extent of the agreement between the calculated and measured P-LLD response for the shallow-flaw specimens.

Figure 6 presents two sets of calculated responses along with the measured responses for the three shallow-flaw specimens (Beams # 38, 37, 26). The measured responses of these specimens appear to indicate the presence of general-yielding conditions at the onset of crack initiation. The two sets of calculated curves correspond to two cases of analysis conditions labeled as Case A and B. The calculated P-LLD curve corresponding to Case A was determined based on a = 10.2 mm and the unadjusted material model. The finite element analysis was carried out under "load-control" in that reaction forces were specified along the back-side of the specimen ahead of the crack tip. Analysis results for Case B were determined based on the actual flaw depth of a = 10.8 mm and the adjusted material model described previously. The finite element analysis was carried out under "displacement-control" as displacements were specified along the back-side of the specimen ahead of the crack tip. As evident from Fig. 6, analysis conditions for Case B appear to result in better agreement between the calculated and measured mechanical responses both in the elastic and plastic regimes.

Comparison for the a/W = 0.5 geometry have been carried out in a similar fashion with details presented by Theiss et al (4). Discrepancies are observed between results based on the unadjusted material model, a/W = 0.5 and the measured responses. Post-test examination of the fracture surfaces for the three deep-flaw specimens indicate that the actual flaw depth is 51.6 mm (a/W = 0.502) rather than the assumed value of 51 mm (a/W = 0.50) or an increase of only 1%. Analysis results determined based on the nominal flaw depth of a/W = 0.50 and the adjusted material model appear to result in better agreement between the calculated and measured mechanical responses both in the elastic and plastic regimes. In subsequent discussions these are referred to as Case D conditions.

## Comparison of Analytical J-Integral Values and J-Estimation Schemes

The J-integral values have been determined as a part of the posttest analysis of the specimens. The magnitude of critical values of P and LLD ($P_c$, $LLD_c$) for the three shallow-flaw specimens at crack initiation are indicated in Table 3. The magnitude of the analytical J-integral based on attaining $LLD_c$ are denoted as $J_{LLDc}$. Since the calculated P-LLD curve for the shallow-flaw specimen underestimates the measured value of LLD at a given value of P, $J_{LLDc}$ can be regarded as an upper bound to the actual value of the J-integral at the onset of crack initiation. On the other hand, the magnitude of the J-integral based on attaining $P_c$ can be regarded as a lower bound to the actual value of the J-integral. These J-integral values are denoted as $J_{Pc}$. Analogous results for the deep-flaw geometry based on Case D conditions are listed in Table 4.

J-estimation schemes based on the magnitude of the experimentally determined LLD and converted from CTOD for both the shallow- and deep-flaw geometry have been presented. The J-integral values based on these estimation schemes, denoted here as $J_{EXP}$ (LLD) and $J_{EXP}$ (CTOD) are listed in Tables 3 and 4 for the shallow and deep-crack beams.

Results in Tables 3 and 4 indicate that both values of $J_{EXP}$ calculated from measured values of LLD compare favourably with the finite element results. The general accuracy of the LLD-based J-estimation scheme for the deep-flaw geometry is verified by the observation that all of the deep-flaw $J_{EXP}$ (LLD) values are between $J_{LLDc}$ and $J_{Pc}$. A similar degree of accuracy is observed for the case of the shallow-flaw geometry, although one of the $J_{EXP}$ (LLD) values is slightly higher than the upper-bound $J_{LLDc}$ value. The J-integral estimation scheme based on CTOD appears to overestimate the fracture toughness for these shallow-flaw specimens since all three values of $J_{EXP}$ (CTOD) were above the upper-bound value of $J_{LLDc}$.

**Table 3 Experimental and analytical results of fracture toughness for the shallow-flaw (a/W = 0.1) specimen based on Case B conditions**

| Beam No. | $P_C$ (kN) | $LLD_C$ (mm) | $JLLD_C$ (kN/m) | $JP_C$ (kN/m) | $J_{EXP}$ (LLD) (kN/m) | $J_{EXP}$ (CTOD) (kN/m) |
|---|---|---|---|---|---|---|
| 38 | 756 | 2.71 | 115 | 112 | 106 | 116 |
| 37 | 746 | 3.08 | 142 | 108 | 135 | 148 |
| 26 | 740 | 3.45 | 169 | 105 | 175 | 201 |

**Table 4 Experimental and analytical results for the fracture toughness for deep-flaw (a/W = 0.5) specimens based on Case D conditions**

| Beam No. | $P_C$ (kN) | $LLD_C$ (mm) | $JLLD_C$ (kN/m) | $JP_C$ (kN/m) | $J_{EXP}$ (LLD) (kN/m) | $J_{EXP}$ (CTOD) (kN/m) |
|---|---|---|---|---|---|---|
| 36 | 176 | 1.24 | 44 | 35 | 35 | 34 |
| 31 | 206 | 1.41 | 57 | 49 | 51 | 53 |
| 25 | 238 | 1.82 | 91 | 71 | 85 | 93 |

## CONCLUSIONS

Several conclusions can be drawn from the results of the HSST shallow-crack fracture toughness program. First, the estimation techniques developed to determine the shallow-crack CTOD and J-integral toughness are valid. Second, the results showed conclusively that A 533 B shallow-flaw beam specimens have a significant increase in CTOD or $J_C$ toughness and $K_C$ toughness in the transition region. Shallow-crack beams had crack depths ranging from 9 to 14 mm (a/W ≈ 0.1 to 0.14), while deep-crack beams had 50 mm deep cracks (a/W ≈ 0.5). Third, little or no difference in toughness on the lower shelf takes place where linear-elastic conditions exist for specimens with either deep or shallow flaws. Next,variations in the beam thickness from 50 to 150 mm had little or no influence on the toughness in both the shallow- and deep-crack specimens. Finally, in the transition region, the increase in shallow-flaw toughness compared with deep-flaw results appears to be well characterized by a temperature shift of 35°C.

## REFERENCES


1. T. J. Theiss, "Recommendations for the Shallow-Crack Fracture Toughness Testing Task Within the HSST Program," USNRC Report NUREG/ CR-5554 (ORNL/TM-11509), August 1990.
2. T. J. Theiss, G. C. Robinson, and S. T. Rolfe, "Preliminary Test Results from the Heavy-Section Steel Technology Shallow-Crack Toughness Program," *Proceedings of the ASME Pressure Vessel & Piping Conference*, Pressure Vessel Integrity, PVP Vol. 213/MPC-Vol. 32, pp. 125–129, ASME 1991.
3. T. J. Theiss and J. W. Bryson, "Influence of Crack Depth on Fracture Toughness of Reactor Pressure Vessel Steel," *Symposium on Constraint Effects in Fracture ASTM STP 1171*, E. M Hackett, K. H. Schwalbe, and R. H. Dodds, Jr., Eds., American Society for Testing and Materials, Philadelphia, (to be published).
4. T. J. Theiss. D. K. M. Shum, and S. T. Rolfe, "Experimental and Analytical Investigation of the Shallow-Flaw Effect in Reactor Pressure Vessels" USNRC Report NUREG/ CR-5886 (ORNL/TM-12115), July 1992.
5. Cheverton, R. D., Iskander. S. K., and Ball, D. G., "Review of Pressurized-Water-Reactor-Related Thermal Shock Studies," *Fracture Mechanics: Nineteenth Symposium, ASTM STP 969*, T. A. Cruse, Ed., American Society for Testing and Materials, Philadelphia, 1988, pp. 752-766.

6. D. J. Naus et al., "SEN Wide-Plate Crack-Arrest Tests Using A 533 Grade B Class 1 Material: WP-CE Series," USNRC Report NUREG/CR-5408 (ORNL/TM-11269), November 1989.
7. D. J. Naus et al., "Crack Arrest Behavior in SEN Wide Plates of Quenched and Tempered A 533 Grade B Steel Tested Under Nonisothermal Conditions," USNRC Report NUREG/CR-4930 (ORNL-6388), August 1987.
8. W. A. Sorem, R. H. Dodds, Jr., and S. T. Rolfe, "An Analytical Comparison of Short Crack and Deep Crack CTOD Fracture Specimens of an A36 Steel," *WRC Bulletin 351*, Welding Research Council, New York, February 1990.
9. J. A. Smith, and S. T. Rolfe, "The Effect of Crack Depth to Width Ratio on the Elastic-Plastic Fracture Toughness of a High-Strength Low-Strain Hardening Steel," *WRC Bulletin 358*, Welding Research Council, New York, November 1990.
10. J. D. G. Sumpter and J. W. Hancock, "Shallow Crack Toughness of HY80 Welds: An Analysis Based on T Stresses," *Int. J. Pres. Ves. & Piping* 45, 207–221 (1991).
11. J. M. Barsom and S. T. Rolfe, *Fracture and Fatigue Control in Structures*, Prentice-Hall, Englewood Cliffs, N.J., 1987.
12. M. T. Kirk, and R. H. Dodds, Jr., "J and CTOD Estimation Equations for Shallow Cracks in Single Edge Notch Bend Specimens," Civil Engineering Studies, Structural Research Series No. 565, Dept. of Civil Engineering, Univ. of Illinois, UILI-ENG-91-2013, Jan. 1991.
13. ABAQUS *Theory Manual*, Version 4-8, Hibbitt, Karlson and Sorensen, Inc., Providence, R.I., 1989.
14. H. Tada, P. C. Paris and G. R. Irwin, *The Stress Analysis of Cracks Handbook*, Del Research Corporation, Hellertown, Pa., 1973.

Fig. 1. Three specimen thicknesses used in the shallow-crack program.

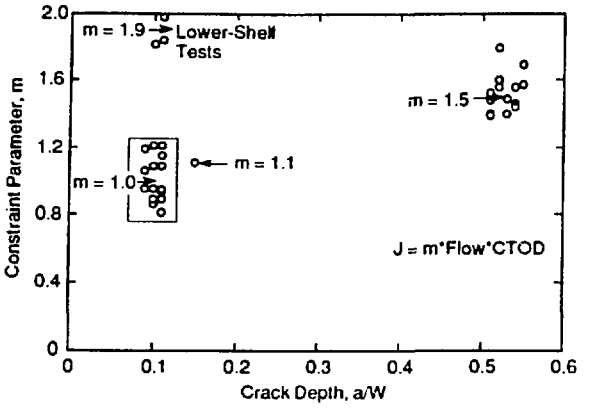


Fig. 2. Constraint parameter (m) values as a function of crack depth (a/W).

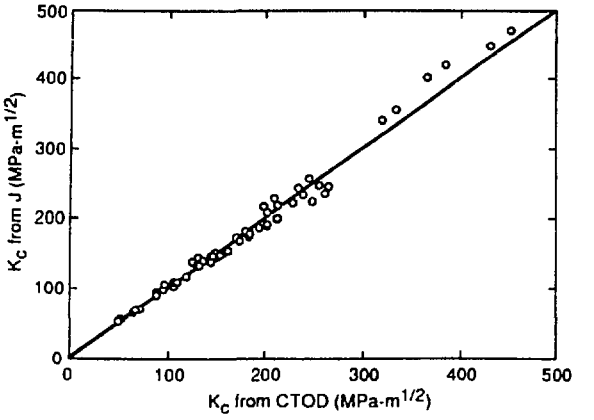


Fig. 3. Comparison of $K_c$ (LLD) and $K_c$ (CTOD) toughness values.

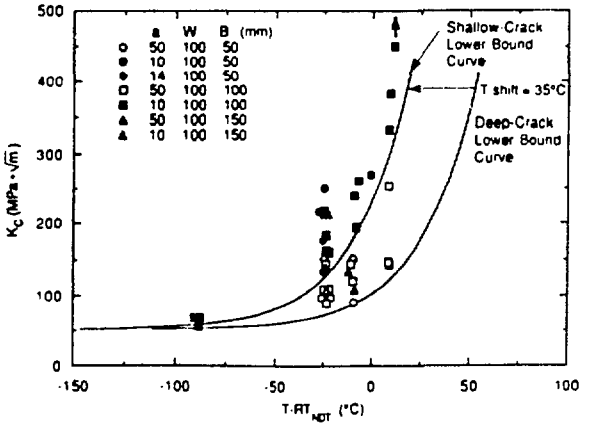


Fig. 4. Toughness ($K_c$) data vs normalized temperature with lower bound curves.

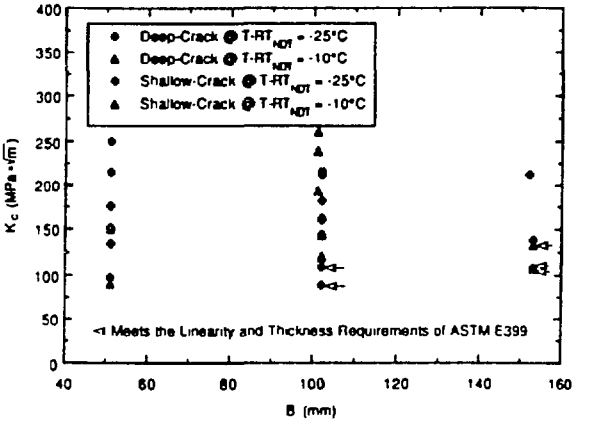


Fig. 5. Toughness ($K_c$) data vs beam thickness at T-RT$_{NDT}$ = –25°C, and –10°C.

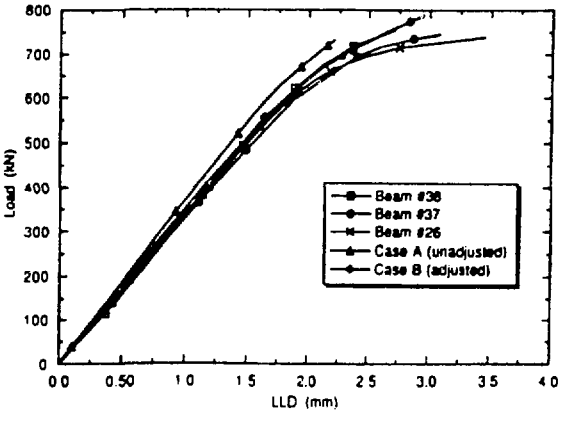


Fig. 6. P-LLD comparison for a/W = 0.1.